Mon. Not. R. astr. Soc. (1969) **143,** 289–300.

THE SPECTRA OF DISCRETE RADIO SOURCES AT DECAMETRIC WAVELENGTHS—I

S. Ya. Braude, O. M. Lebedeva, A. V. Megn,
B. P. Ryabov and I. N. Zhouck

(Received 1968 August 19)

SUMMARY

The present paper describes the methods used and the results of measurements made on 80 discrete radio source spectra in the decametric wavelength range. Flux densities are given for frequencies 12·6 MHz, 14·7 MHz, 16·7 MHz, 20 MHz and 25 MHz.

INTRODUCTION

The basic data on flux densities and spectra of discrete radio sources observed in the northern hemisphere have mostly been obtained at frequencies above 30 MHz. At longer wavelengths, radio source spectra have been studied previously only in a comparatively small number of cases (**1**)–(**9**) because of the influence of the ionosphere, the high cosmic background level and also because of various kinds of radio interference which are especially important for low resolving power instruments.

The present paper gives the results of measurements of the spectra of 80 discrete radio sources at frequencies from 12·5 to 25 MHz, obtained with a radio telescope UTR-1 in the Institute of Radiophysics and Electronics of the Ukrainian Academy of Science in Grakovo during the period 1966–68.*

EQUIPMENT AND METHOD OF OBSERVATION

The radio telescope UTR-1 comprises two arrays consisting of wideband horizontal dipoles positioned in the form of a letter T. One of the arrays is 600 m in length, and comprises 80 dipoles in a single row. This array is oriented along the N–S direction. The second array is 576 m in length, and comprises 128 dipoles in two rows along the E–W direction.

The radio telescope operates over the frequency range 10–25 MHz and the maximum effective area of each of the arrays is near 14 000 m^2. Antenna beam control of the radio telescope in declination and right ascension is made electrically by the use of three phasing systems, two being used for array signal phasing and the third for reciprocal signal phasing between the arrays. Signals are detected by a switched radiometer system, providing in a zenith direction a resulting half-power beam width which varies from $40' \times 1^\circ 30'$ to $1^\circ 40' \times 3^\circ 45'$ at maximum and minimum frequency respectively. The radio telescope block-diagram is given in Fig. 1. The output signal of each array is fed to preliminary radio frequency amplifiers (RFPA) designed to provide an optimum noise-factor simultaneously with the complete absence of cross-modulation interference. In multi-channel

* Preliminary results of this paper were reported to Commission 40 of the I.A.U. at the 13th General Assembly in Prague on 29th August 1967.

reception, the use of these amplifiers allows a number of channels to be used independently; it also removes the effects of feeder loss and of noise in the radiometer input circuits. From the RFPA output, the signals are fed via cables and the reciprocal antenna phasing system to the wideband phase modulator (0–π) which

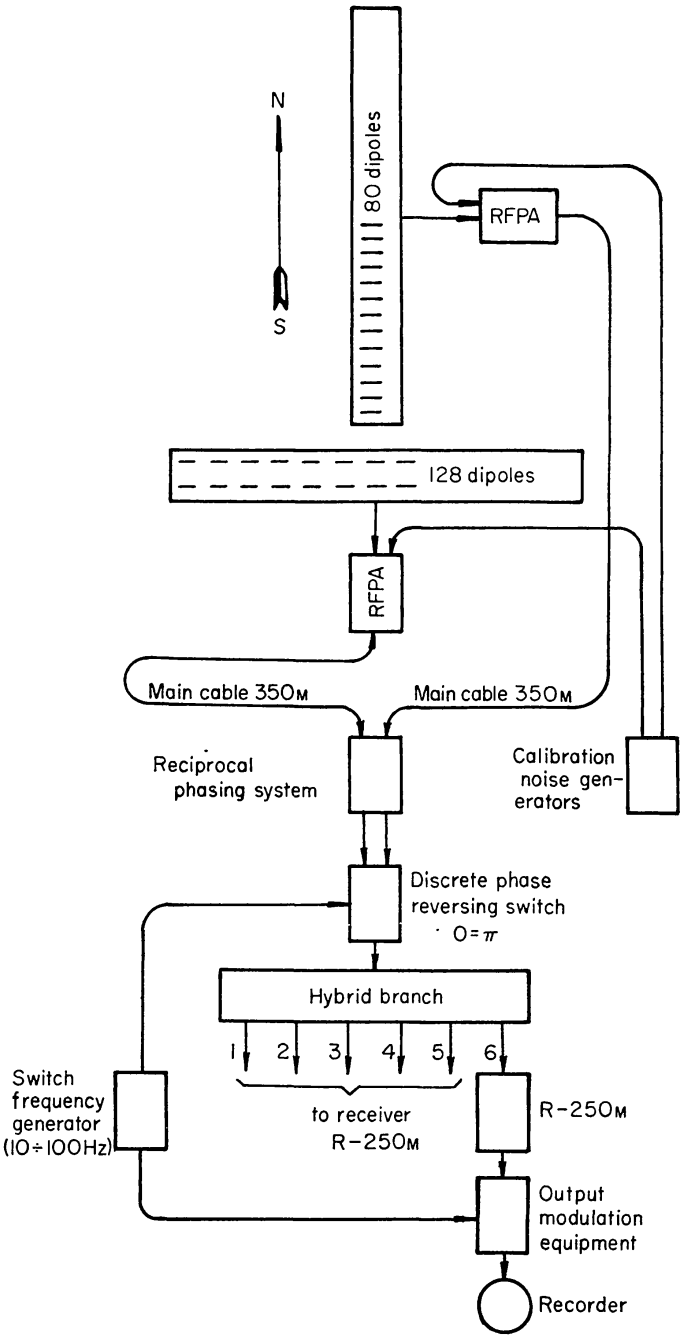

FIG. 1. *Block diagram of radio telescope UTR-1.*

switches a signal phase of one of the antennae at a frequency between 10 and 100 Hz by diode switches. In the phase modulator, the elimination of spurious amplitude modulation and the precision of the 180° phase shift over the whole of the frequency range is achieved by a multicascade symmetrizing circuit with wideband ferrite transformers. This circuit, with careful selection of diodes, ensures an amplitude

asymmetry less than 0·2 per cent, and a phase error not larger than one or two degrees. After the phase modulator, the signals from both antennae are added in a hybrid circuit. To eliminate any spurious modulation of background noise, the cross-modulation between channels is kept below −40 db. throughout. From the hybrid output, the signals are fed via branching hybrids to six radiometers operating at various frequencies. Each radiometer includes an R-250 M-type receiver and a highly stable detector of the modulated output, used for filtering, amplification and recording of signals at the phase modulation frequency.

The wideband phase modulator generates harmonics and sidebands of strong interfering signals, due to the pulse modulation at the time of switching. The effects of this were completely removed by switching the gain of the intermediate frequency amplifiers to zero by a pulse derived from the drive of the phase modulator. The pulse width conforms with the bandwidth of the intermediate frequency amplifier (IFA), which was set between 3 and 14 kHz depending on the interference level. When strong interference was present, the lowest bandwidth and the lowest switch frequency were used.

To make the amplification of modulated signals independent of the background level, the radiometers have precise linear power characteristics. The calibration has been found to be independent of an artificially added background level over a range of 28 db. The signal reception was made at five various frequencies simultaneously: 12·6 MHz, 14·7 MHz, 16·7 MHz, 20 MHz, 25 MHz and in some cases at 10 MHz as well. Because of the high level of interfering signals and the presence of ionospheric absorption during the day, measurements were made mainly at night. To achieve a high stability and precision of measurement, the radio telescope equipment was operated continuously and a radiometer calibration was made twice during each night. Furthermore, all radiometers were equipped with automatic gain control for the R-250 M-type receivers which included a reference high temperature diode noise generator, a high frequency diode switch and AGC amplifiers. Noise diode signals were from time to time connected to six radiometer inputs via a high frequency switch and a hybrid branch. In this case, the radiometer outputs are connected with individual AGC amplifiers thereby ensuring a proper gain control. The high frequency switch system cuts off the receiver inputs from the radio telescope antennae simultaneously, and at the same time the switching pulse which sets the amplifier gain to zero is removed. The reference signals are synchronized with the moment of switching of the phase modulator diodes, so that the switching occurs at twice the frequency of the phase modulation. Such a synchronization proved to be quite useful for the elimination of interference arising when a phase modulator is in operation.

Such equipment together with fast radiometer retuning provided reliable protection from interference during measurements at night. During each night of observation, one could usually record about 10 radio sources each of 40^m–$1^h\,30^m$ duration. The integration time constant was adjusted from 120 to 225 s, depending on the frequency, to obtain the best output signal-to-noise ratio.

The equipment calibration was made by the phase switching method using a standard noise generator (SNG). The signals from SNG were fed via a hybrid circuit and additional cables to the amplifier inputs at the antennae (Fig. 1). Random variations of the output from these calibration signals due to radiometer gain instability and random SNG errors, together with other calibration errors were usually of the order of 0·4 to 0·6 db.

As the preliminary data in the dacametric wavelength range show, there are, probably, variations in intensity of radiation from some intense sources used for comparison with those being measured. Furthermore, the parameters for an antenna with electrical beam control are functions of beam orientation. The flux density S of discrete sources of radiation was therefore found by an absolute method by the standardization of all the parameters of the radio telescope.

The recorded signal power P from a discrete source with flux density S is given by

$$S = \frac{2P}{A\eta k}.$$

In this expression A and η are the effective area and the efficiency of the radio telescope antenna and k is a coefficient due to reduction of the signal in the integrating circuit of the detector.

In order to determine an effective area and the efficiency of the array, the results of antenna measurements given in (**10**), (**11**) were used. In determining the value of A, the antenna array directivity was included together with real ground parameters. Factors reducing A, such as random phase and amplitude deviations of different antenna elements, exponential current amplitude distribution along the antennae and phase current errors because of discrete control of beam position, were also allowed for. In calculating the efficiency, due account was taken of losses in the antenna and phase systems. In the process of evaluation of the antenna efficiency (on the basis of Ref. (**12**)), there were taken into account two types of surface parameters corresponding to dry ($\epsilon' = 4-j2$) and wet ground conditions ($\epsilon' = 10-j10$). The observed decrease of record amplitude due to integration was found both theoretically and experimentally, leading to values of k given by the empirical expression:

$$k = 1/(1+0{\cdot}66(\psi\tau)^2-0{\cdot}06(\psi\tau)^3)^{1/2} \qquad \psi = (\pi nd\Omega/\lambda)\cos\delta$$

where τ is integration time constant, δ is the declination of the source, Ω is angular rotational velocity of the Earth, n and d are the number of dipoles and the distance between two successive dipoles in the W–E direction and λ is the wavelength.

The precision of the observations described was limited mainly by errors of measurement, by errors in the evaluation of the effective area and the efficiency (because of uncertainty in the ground parameters and other antenna parameters, the standard deviation is < 13 per cent) and errors of determination of spectral density of SNG ($\leqslant 7$ per cent). Besides random errors and equipment instability, there must be added to the errors of measurement the effect of variations in the ionospheric absorption coefficient which at night and even at the lowest frequency did not exceed 0·2–0·3 db. When interference was important, the error was increased by the maximum magnitude of parasitic signals.

The minimum level of measurable signals was determined by the side lobe scattered radiation level rather than by the width of the main lobe of the response pattern.

The resulting measurement error shown in the figures and tables was determined as the sum of the systematic error and the standard deviation of the random error. All the measurements were repeated until the standard deviation became less than 5–10 per cent.

Table I

Spectral flux densities, S (10^{-24} W m^{-2} Hz^{-1})

	Source number	α(1950)	δ(1950)	MHz	12·6		14·7		16·7		20		25		Spectral index		
					S	±ΔS%	S	±ΔS%	S	±ΔS%	S	±ΔS%	S	±ΔS%	α_{hf}*	α_{hf}	α_{lf}
1	3C 9	00h17m50·2s	15°24·8′						2·5	38	1·7	27	1·9	17	0·9 [16]	1·02	
2	3C 10	00 22 40·7	63 54·1		10·8	52	9·5	26	9·6	27	9	22			0·67 [19]	0·67	
3	3C 28	00 53 09·6	26 09·7		6·5	49	3·9	45	2·7	45	2·4	39	1·8	31	1·13 [19]	1·13	1·6
4	3C 33	01 06 13·8	13 04·5		4·6	33	4·0	23	3·4	21	2·3	16	2·8	13	0·71 [19]	0·76	
5	3C 34	01 07 33·5	31 31·2		5·4	56	3·1	48	2·5	41	2·0	39	1·1	28	1·07 [20]	1·03	2·0
6	3C 47	01 33 40·1	20 43·2		5·9	34	5·1	32	3·2	19	2·9	17	2·1	17	0·89 [19]	1·02	
7	3C 48	01 34 49·9	32 53·5										0·62	20	0·52 [19]	0·52	
8	3C 55	01 54 20·1	28 35·8		3·9	32	2·6	24	2·1	26	1·8	21	2·0	18	0·94 [19]	1·02	
9	3C 65+																
	4C 39·6	02 20 36·9	39 47·9		3·7	47	2·3	32	1·8	40	1·2	30	0·97	31	1·05 [19]		
10	3C 66	02 20 09·1	42 48·1		6·8	31	4·3	28	3·3	23	2·5	20			0·71 [19]	0·67	1·7
11	3C 75	02 55 02·5	06 00·4		12	20	5·4	17	5·9	23	3·1	19	2·0	17	0·73 [19]	0·67	2·5
12	3C 79	03 07 11·6	16 54·3		4	27	2·9	21	2·1	17	2·4	16	1·6	19	0·80 [19]	0·92	
13	3C 84	03 16 28·6	41 19·8		19	13	16·7	13	15·5	14	10·8	13	10·5	13	0·62 [19]	0·62	1·42
14	3C 89	03 31 41·1	−01 23·5		11·7	15	5·4	18	4·0	18	2·4	15	1·9	19	0·79 [19]	1·02	1·92
15	3C 98	03 56 11·0	10 17·2		8·8	24	4·8	23	4·2	19	3·9	17	2·6	20	0·74 [19]	0·81	1·42
16	3C 103	04 04 35·3	42 52·6		3·1	23	2·8	21	2·5	18	2·2	17	2·1	17	0·88 [19]	0·89	
17	3C 109	04 10 55·0	11 05·8		5·8	35	3·5	25	2·9	19	1·9	17	1·4	15	0·81 [19]	0·85	1·82
18	3C 111	04 15 01·7	37 53·9		6·0	15	5·3	14	4·7	15	4·1	14	4·6	14	0·74 [19]	0·79	
19	3C 123	04 33 55·1	29 34·4		12·8	14	10·9	14	8·8	14	10·8	15	11	16	0·74 [19]	0·78	
20	3C 125	04 42 50·9	39 40·0		3·6	44	2	33	1·7	23	1·2	25	1·15	22	0·89 [20]	0·92	1·52
21	3C 129+																
	3C 129(1)	04 45 24·8	44 56·5		8·1	17	5·6	20	3·3	16	3·6	15	3·2	14	0·78 [15]	0·78	1·50
22	3C 130	04 48 53·3	52 00·2		6·8	30	2·9	27	2·2	22	1·5	23	1·35	23	0·84 [15]	0·93	1·55
23	3C 134	05 01 17·8	38 02·2		10·1	14	9·8	15	7·0	16	6·0	14	5·7	14	1·0 [19]	1·02	
24	3C 139(2)	05 21 19·2	28 10·5				2·6	37			1·3	37	1·3	14	0·81 [20]	1·08	
25	3C 141	05 23 27·2	32 47·6				3·0	33	2·1	25	1·5	20	1·7	26	0·87 [19]	1·06	

TABLE I (*continued*)

Spectral flux densities S (10^{-24} *W m*$^{-2}$ *Hz*$^{-1}$)

	Source number	α(1950)	δ(1950)	MHz	12·6		14·7		16·7		20		25		Spectral index		
					S	±Δ*S*%	*S*	±Δ*S*%	*S*	±Δ*S*%	*S*	±Δ*S*%	*S*	±Δ*S*%	α_{hf}*	α_{hf}	α_{lf}
26	3C 142(1)	05h28m47·7s	06° 29·2′						3·3	49	1·4	39	1·35	39	0·79 [19]	0·93	
27	3C 144	05 31 30	21 58·4	53		15	53	15	38·3	14	31·7	14	34·2	14	0·26 [19]	0·26	0·86
28	3C 152	06 01 30·1	20 21·8						1·8	38	1·3	20	0·9	22	0·72 [20]	1·04	
29	3C 153	06 05 44·5	48 05·0	2·1		20	1·6	20	1·3	16	1·0	17	0·8	16	0·80 [19]	0·71	1·34
30	3C 154	06 10 43·5	26 06·0	3·9		22	3·1	32	2·2	33	2·3	22	1·6	20	0·76 [19]	0·91	
31	3C 157	06 14 36	22 43								6·0	24	6·3	21	0·30 [19]	0·33	
32	3C 161	06 24 42·3	−05 48·0	5·6		24	4·3	24	3·2	16	2·7	16			0·61 [19]	0·63	1·12
33	3C 166	06 42 23·9	21 26·8	3·2		28	3·0	24	1·8	18	1·6	20	1·4	18	0·90 [19]	0·98	
34	3C 171	06 51 10·4	54 14·1	3·1		25	1·8	22	1·6	20	1·6	20			0·95 [19]	0·84	
35	3C 174	07 05 27·4	−07 54·1						2·6	18	1·6	19	0·9	17	1·14 [15]	1·0	2·83
36	3C 175	07 10 16·1	11 49·6	4·0		24	4·3	19	2·8	17	2·2	16			0·97 [19]	0·92	1·42
37	3C 191	08 02 03·9	10 22·5	3·8		22	3·0	22	1·6	20	1·2	15	0·8	15	0·98 [19]	0·98	1·79
38	3C 192	08 02 36·2	24 17·6						2·3	16	2·3	14	1·9	14	0·75 [19]	0·82	1·2
39	3C 196	08 09 59·6	48 44·3	4·5		17	3·7	14	3·1	14	3·1	14	3·1	14	0·73 [19]	0·76	
40	3C 196(1)	08 12 56·6	−02 59·1	4·6		30	3·7	28	3·7	21	2·9	22			1·1 [16]	1·16	
41	3C 200	08 24 21·8	29 28·9						1·2	23	1·0	22	0·9	17	0·77 [20]	0·91	
42	3C 208+																
	3C 208(1)	08 50 22·9	14 04·0	3·9		46	3·1	39	2·4	33	2·3	30	2·0	31	0·81 [19]	0·97	
43	3C 216	09 06 17·7	43 03·5	2·4		40	1·4	37	1·5	34	1·1	25	1·1	17	0·83 [19]	0·82	
44	3C 218	09 15 40·8	−11 53·0	39		16	30	15	30	14	21·5	15			0·93 [19]	0·97	
45	3C 219	09 17 50·2	45 51·7	4·4		16	4·0	14	2·9	14	2·2	16			0·80 [19]	0·87	
46	3C 227	09 45 08·0	07 39·8	5·7		18	3·7	16	3·7	16	3·2	16			0·82 [19]	0·89	
47	3C 228	09 47 27·9	14 33·6	5·4		33	2·7	24	1·9	20	1·5	24	0·9	18	0·86 [19]	0·82	1·8
48	3C 234	09 58 57·1	29 00·9	6·8		18	5·6	16	3·1	15	3·3	15			0·85 [19]	0·91	1·7
49	3C 238	10 08 22·7	06 39·2						2·0	34	1·7	33	1·3	41	0·69 [19]	0·97	
50	3C 239	10 08 39·1	46 43·0	2·6		28	1·8	27	1·7	24	1·1	21	1·4	18	1·12 [15]	1·07	
51	3C 244(1)	10 30 20·2	58 29·2				1·8	16	1·5	15	1·2	14	1·1	15	0·95 [15]	0·84	
52	3C 250	11 06 11·4	25 14·0	3·8		20	2·7	15	2·0	19	1·5	28	1·7	52	0·98 [20]	1·22	

TABLE I (*continued*)

Spectral flux densities S (10^{-24} $W\,m^{-2}\,Hz^{-1}$)

	Source number	α(1950)	δ(1950)	MHz	12·6		14·7		16·7		20		25		Spectral index		
					S	$\pm\Delta S$%	S	$\pm\Delta S$%	S	$\pm\Delta S$%	S	$\pm\Delta S$%	S	$\pm\Delta S$%	α_{hf}*	α_{hf}	α_{lf}
53	3C 252	$11^h08^m48{\cdot}2^s$	35° 55·0′		2·8	57	2·1	38	1·8	25	1·7	24			1·08 [20]	1·15	
54	3C 254	11 11 52·7	40 53·7		1·95	46	2·1	30	1·4	20	1·3	22	1·1	18	0·93 [19]	1·05	
55	3C 264	11 42 31·1	19 53·3		14·4	41	5·3	22	3·8	17	3·1	16			0·78 [19]	0·85	1·5
56	3C 265	11 42 53·0	31 50·4						3·0	18	1·9	17	1·7	43	0·92 [19]	1·02	
57	3C 270	12 16 37·5	06 06·3								2·9	21	2·2	27	0·50 [19]	0·54	1·33
58	3C 273	12 26 32·8	02 17·6						5·8	37	6·7	28	8·6	43	0·40 [19]	0·32	1·42
59	3C 274	12 28 18·0	12 40·1		91	14	87·5	14	77	14	60·5	14	53	14	0·82 [19]	0·82	
60	3C 280	12 54 41·6	47 36·2		2·5	31	1·8	30	1·7	28	1·4	24	1·3	21	0·73 [19]	0·82	
61	3C 287	13 28 16·7	25 23·9		3·2	50	2·4	50	1·4	44	1·2	42	0·65	32	0·48 [19]	0·52	1·86
62	3C 295	14 09 33·8	52 23·5		2·9	28	1·9	20	1·5	19	1·1	18	1·6	16	0·58 [19]	0·68	1·92
63	3C 298	14 16 38·7	06 43·0						1·5	21	1·3	18	1·0	16	0·98 [19]	1·02	
64	3C 310	15 02 48·9	26 12·5		8·2	15	6·4	18	4·9	14	4·4	16	4·1	16	1·0 [19]	1·0	
65	3C 313	15 08 32·8	08 02·5						2·7	41	3·0	23			0·87 [19]	0·99	
66	3C 321	15 29 40·6	24 13·2						1·7	20	1·7	15	1·0	16	0·70 [20]	0·85	
67	3C 327	15 59 59·0	02 05·0		11	25	7·4	21	5·3	16	5·4	15			0·85 [19]	0·89	1·32
68	3C 338	16 26 55·3	39 39·3		7·9	18	5·4	19	3·4	15	2·5	15	2·6	14	1·17 [19]	1·21	
69	3C 348	16 48 40·3	05 03·8		63·5	14	60	14	42	14	36·5	14	23	13	0·98 [19]	1·04	
70	3C 353	17 17 56·1	−00 57·0		19	17	16·7	17	15·5	13	10·9	13	11·5	13	0·70 [19]	0·73	
71	3C 380	18 28 14·0	48 42·3						4·7	19	3·3	20			0·77 [19]	0·78	
72	3C 382	18 33 13·2	32 38·6				4·2	38	3·3	34	2·2	24			0·69 [19]	0·77	1·72
73	3C 405	19 57 45·3	40 36·0	219		15	317	15	266	14	270	14	315	14	0·80 [19]		
74	3C 461	23 21 10·6	58 33·1	585		14	650	14	600	14	650	14	580	14	0·77 [19]	0·77	
75	4C 24·15	07 26 27·3	24 42·9		3·1	17	2·7	19	2·0	19	1·2	19	1·1	15	1·16 [21]	1·41	
76	4C 21·23	07 36 50·8	21 01·7		3·5	40	2·0	28	1·7	20	1·0	25	0·64	27	0·99 [21]	1·18	2·5
77	4C 38·27	09 08 53·8	38 03·0						2·3	53	1·5	47	1·8	44	1·19 [15]	1·15	
78	4C 14·31	09 22 22·6	14 57·4		2·9	36	2·7	20	1·7	21	1·8	27	0·63	24	1·0 [16]	1·09	2·1
79	4C 38·39	14 24 03·9	38 01·2						1·5	16	1·1	17	0·84	16	1·55 [21]	1·55	
80	NRAO 416	12 56 59	28 10·3		6·9	32	5·2	33	3·6	28	2·9	19	3·0	17	1·68 [15]	1·48	

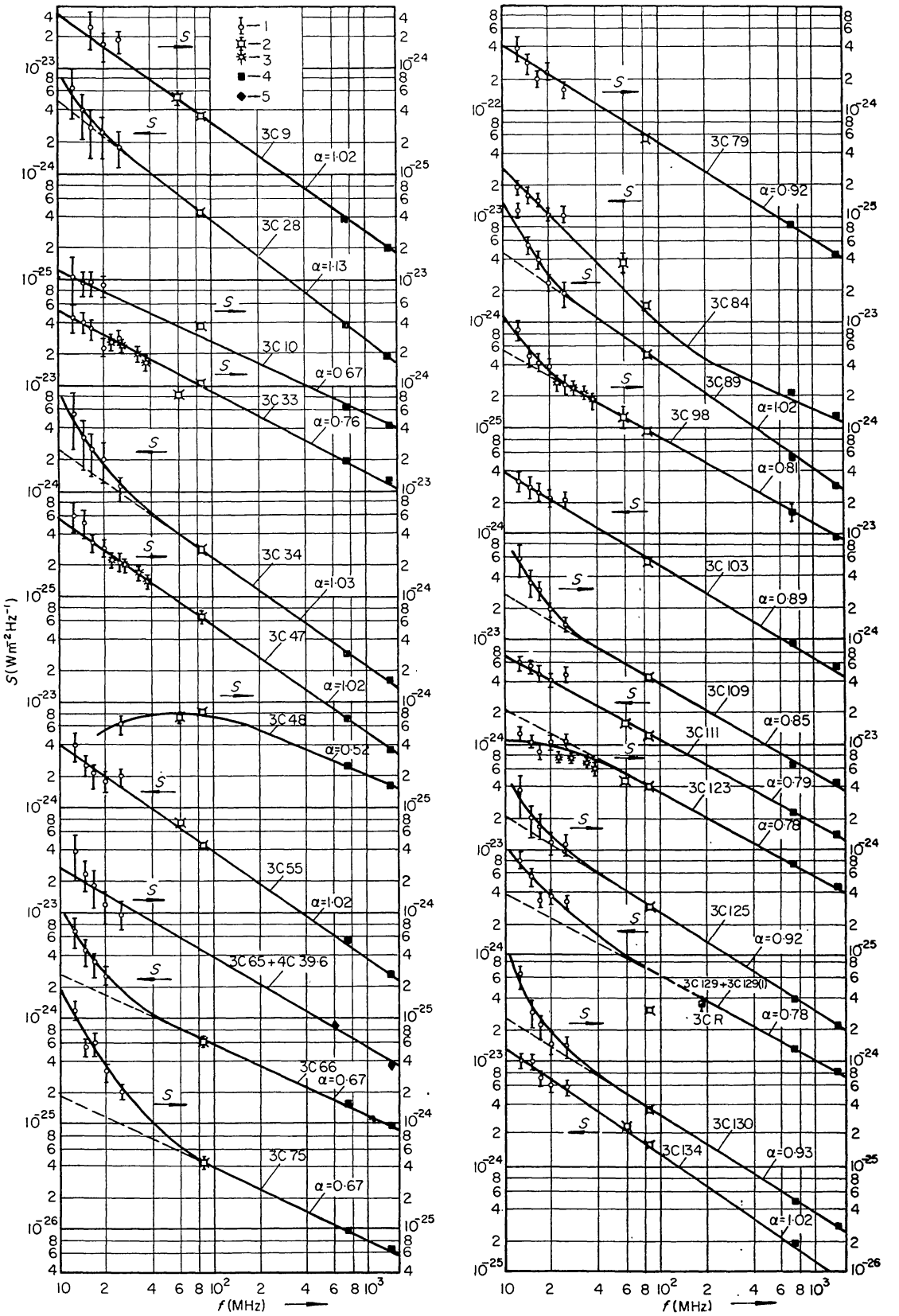

FIG. 2(a). *Spectra of the radio sources.*

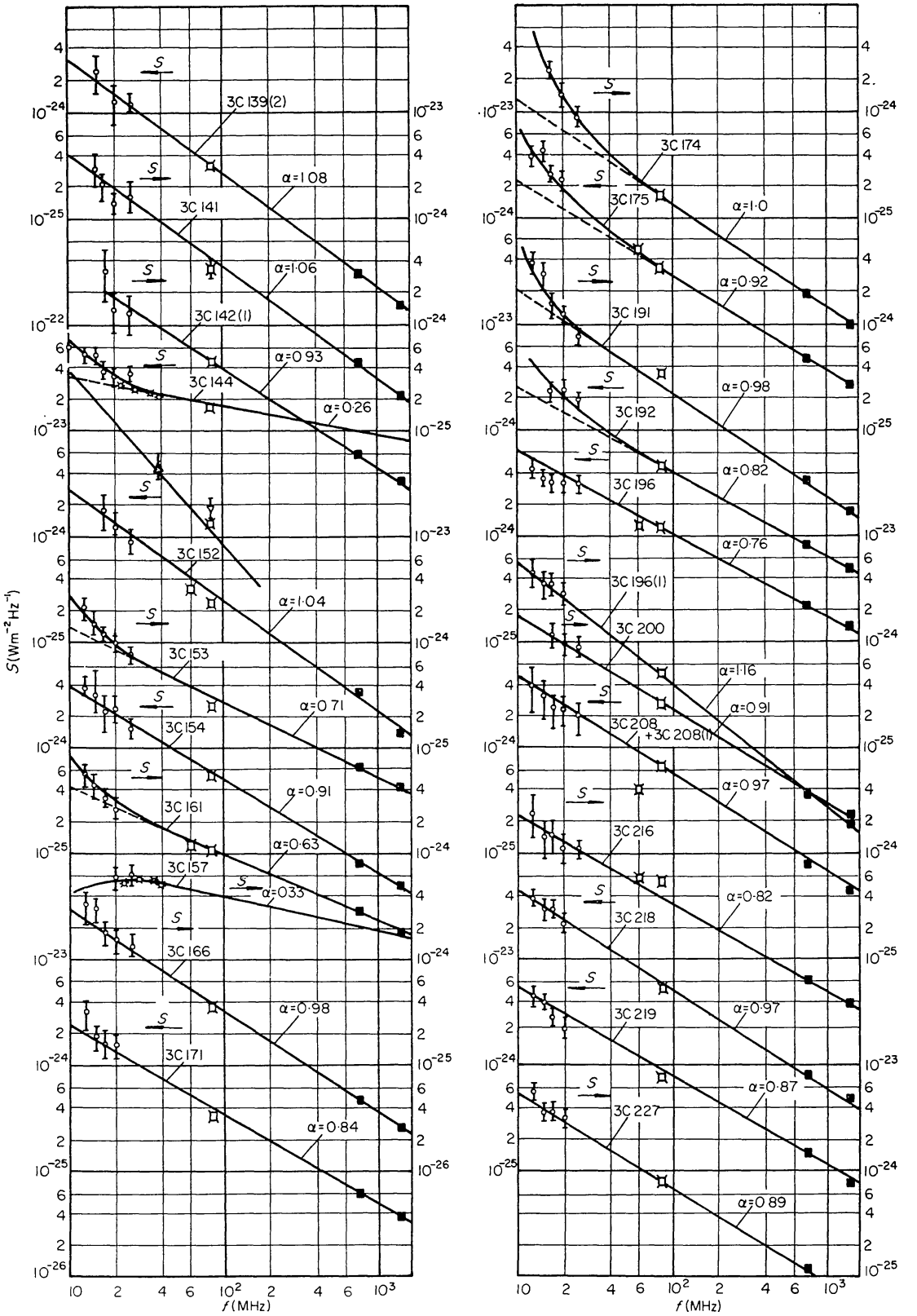

FIG. 2(b). *Spectra of the radio sources.*

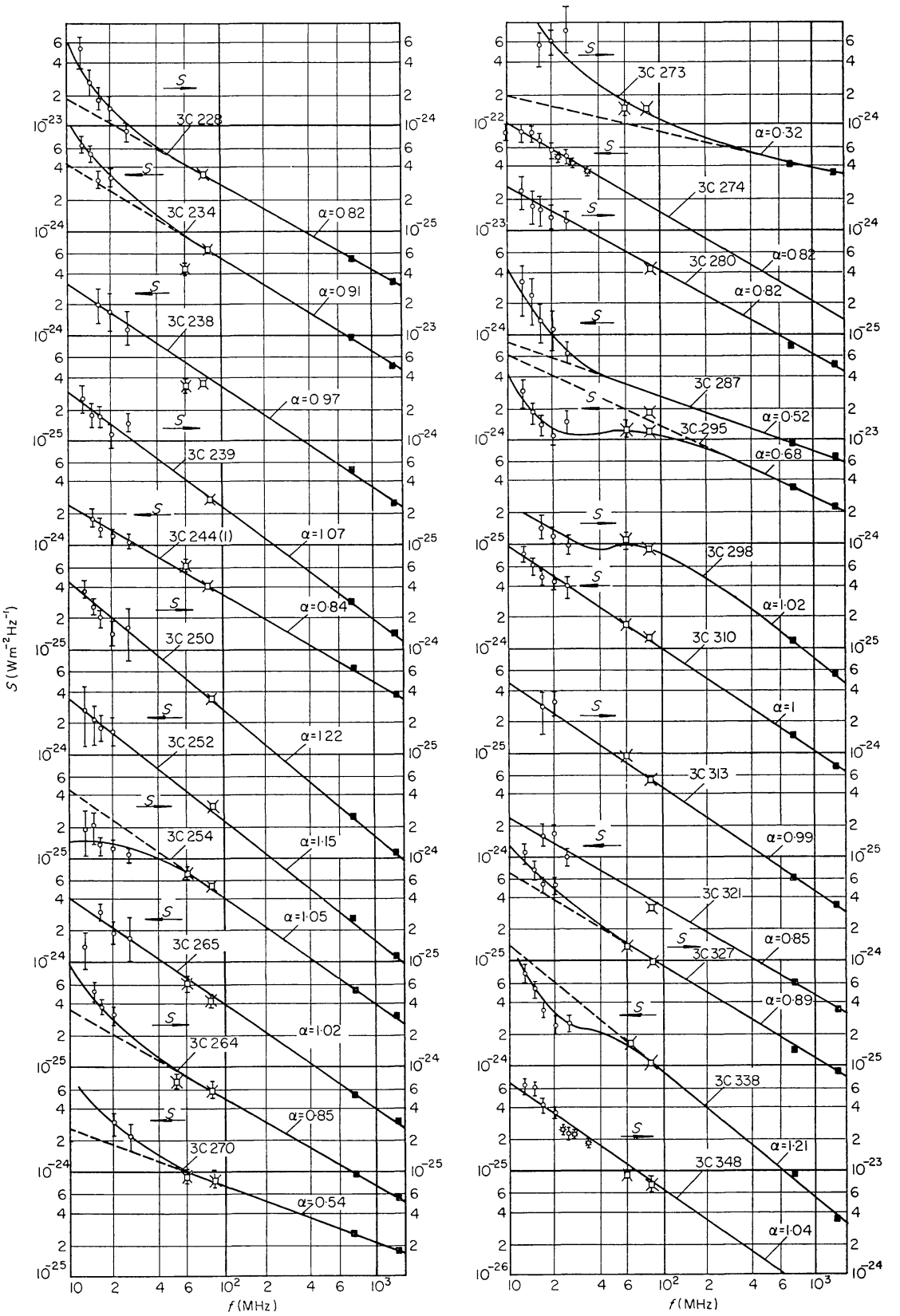

FIG. 2(c). *Spectra of the radio sources.*

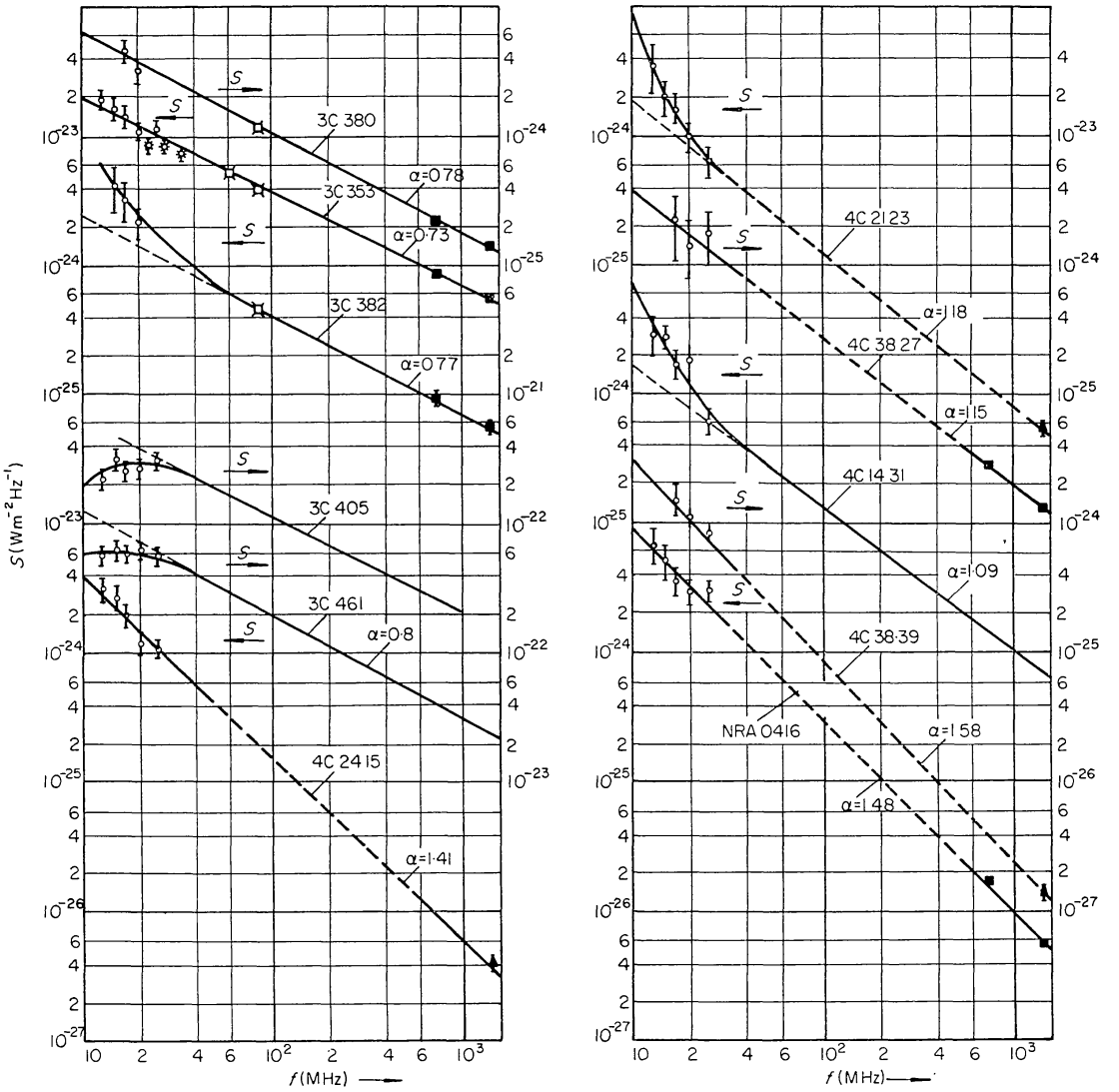

FIG. 2(d). *Spectra of the radio sources.*

THE RESULTS OF THE MEASUREMENTS

The basic results of the measurements are given in Table I which gives spectral flux densities S in 10^{-24} W m^{-2} Hz^{-1} and the resulting percentage error ΔS for five frequencies from 12·6 to 25 MHz. Designations and co-ordinates of sources except for some particular cases correspond to those given in catalogues (**13**)–(**15**). For the sources 3C 144, 3C 274 and NRAO 416, the flux density was also measured at 10 MHz. Their values in units of 10^{-24} W m^{-2} Hz^{-1} are equal to 66, 90 and 127 with percentage errors of 29, 18 and 32 respectively. The results obtained in the decametric wavelength range together with those taken from the literature (**1**)–(**9**), (**15**)–(**22**) allow us to represent the source spectra in detail. Furthermore, in certain cases it is possible to specify spectral features of the observed sources in a much wider range from 12 to 1000–3000 MHz. In Fig. 2 such spectra are shown on a logarithmic scale. On the basis of these plots, drawn by the method of least squares, the spectral indices α_{lf} and α_{hf} were determined respectively at low (i.e. < 30 MHz) and high (i.e. > 30 MHz) frequencies. For comparison purposes in Table I, indices α_{hf}* determined by Kellerman (**19**) and other authors (**15**), (**16**), (**20**), (**21**) are given.

From the data shown, it is evident that in the decametric range the spectral parameter essentially differs from that typical of the synchrotron radiation mechanism for which $S \sim f^{-\alpha_{hf}}$.

The spectra of the radio sources may be classified in four groups as follows. The first two groups, already known from the literature (2), (4), (8), include logarithmically linear spectra having $\alpha_{lf} = \alpha_{hf}$ and those with negative curvature. The third type involves spectra with positive curvature when the spectral index α increases with decreasing frequency. Finally there are some radio sources with more complicated spectra. These sources have spectral regions with both positive and negative curvature. A detailed analysis of all these types of spectral characteristics will be made in the following paper (Part II).

ACKNOWLEDGMENTS

In conclusion, the authors would like to thank L. G. Sodin and Ju. M. Bruck for their contribution to the design of the receiving equipment and the determination of the array parameters.

REFERENCES

(1) Roger, R. S., Costain, C. H. & Purton, C. R., 1965. *Nature, Lond.*, **207,** 62.
(2) Ericson, W. C. & Cronyn, W. M., 1965. *Astrophys. J.*, **142,** 1157.
(3) Clark, T. A., 1966. *Astr. J.*, **71,** 158.
(4) Andrew, B. H., 1967. *Astrophys. J.*, **147,** 423.
(5) Bridle, A. H., 1967. *Observatory*, **87,** 60.
(6) Guidice, D. A., 1966. *Nature, Lond.*, **211,** 57.
(7) Bazelyan, L. L., Braude, S. Ya., Bruck, Yu. M., Zhouck, I. N., Megn, A. V., Ryabov, B. P., Sodin, L. G. & Sharykin, N. K., 1963. *Radiofiz.*, **6,** 897.
(8) Bazelyan, L. L., Braude, S. Ya., Vaisberg, V. V., Krymkin, V. V., Megn, A. V. & Sodin, L. G., 1965. *Astr. Zh.*, **42,** 618.
(9) Bazelyan, L. L., Braude, S. Ya. & Megn, A. V., 1966. *Astr. Cirk.*, No. 357.
(10) Bruck, Yu. M., Goncharov, N. Yu., Megn, A. V., Sodin, L. G., Sharykin, N. K., 1967. *Radiofiz.*, **10,** 608.
(11) Bruck, Yu M., Goncharov, N. Yu., Zhouck, I. N., Inyutin, G. I., Megn, A. V., Sodin, L. G. & Sharykin, N. K., 1968. *Radiofiz.*, **II,** 28.
(12) Sodin, L. G., 1968. *Radiofiz.***II**, , 101.
(13) Bennett, A. S., 1962. *Mem. R. astr. Soc.*, **68,** 163.
(14) Pilkington, J. D. H. & Scott, P. F., 1965. *Mem. R. astr. Soc.*, **69,** 183; Gower, J. F. R., Scott, P. F. & Wills, D., 1967. *Mem. R. astr. Soc.*, **71,** 49.
(15) Pauliny-Toth, I. I. K., Wade, C. M. & Heeschen, D. S., 1966. *Astrophys. J., Suppl. Ser.*, **13,** 65.
(16) Day, G. A., Shimmins, A. J., Ekers, R. D. & Cole, D. J., 1966. *Aust. J. Phys.*, **19,** 35; Shimmins, A. J., Day, G. A., Ekers, R. D. & Cole, D. J., 1966. *Aust. J. Phys.*, **19,** 837.
(17) Williams, P. J. S., Kenderdine, S. & Baldwin, J. E., 1966. *Mem. R. astr. Soc.*, **70,** 53.
(18) Artyukh, V. S., Vitkevich, V. V., Dagkesamanskii, R. D. & Koshukhov, V. N., 1967. Preprint No. 82, Lebedev Physics Institute, Academy of Sciences, U.S.S.R.
(19) Kellerman, K. I., 1964. *Astrophys. J.*, **140,** 969.
(20) Long, R. J., Smith, M. A., Stewart, P. & Williams, P. J. S., 1966. *Mon. Not. R. astr. Soc.*, **134,** 371.
(21) Olsen, E. T., 1967. *Astr. J.*, **72,** 738.
(22) Aslanian, A. M., Dagkesemanskii, R. D., Kozhukhov, V. N., Malumian, V. G. & Sanamian V. A., 1968. *Astrofiz.*, **4,** 129.